Analytical and Bioanalytical Chemistry (2019) 411:5509–5518
https://doi.org/10.1007/s00216-019-01929-5

RESEARCH PAPER

Gold-nanorod-enhanced Raman spectroscopy encoded micro-quartz pieces for the multiplex detection of biomolecules

Bei Wang[1] · Tian Guan[2] · Jingying Jiang[3,4] · Qinghua He[2] · Xuejing Chen[2] · Guangxia Feng[2] · Bangrong Lu[2] · Xuesi Zhou[2] · Yonghong He[2]

Received: 28 March 2019 / Revised: 8 May 2019 / Accepted: 16 May 2019 / Published online: 6 July 2019

Abstract

The rapid analysis and detection of biomolecules has become increasingly important in biological research. Hence, here we propose a novel suspension array method that is based on gold nanorod (AuNR)-enhanced Raman spectroscopy and uses micro-quartz pieces (MQPs) as microcarriers. AuNRs and Raman reporter molecules are coupled together by Au–S bonds to obtain surface-enhanced Raman scattering labels (SERS labels). The SERS labels are then assembled on the surfaces of the MQPs via electrostatic interactions, yielding encoded MQPs. Experimental results showed that the encoded MQPs could be decoded using a Raman spectrometer. A multiplex immunoassay experiment demonstrated the validity and specificity of these encoded MQPs when they were used for bioanalysis. In concentration gradient experiments, the proposed method was found to give a linear concentration response to the target biomolecule at target concentrations of 0.46875–30 nM, and the detection limit was calculated to be 1.78 nM. The proposed method utilizes MQPs as carriers rather than conventional microbeads, which allows the interference caused by the background fluorescence of microbeads to be eliminated. The fluorescence of the encoded MQPs can be simply, rapidly, and inexpensively quantified using fluorescence microscopy. By dividing the quantitative and qualitative detection of biomolecules into two independent channels, crosstalk between the encoded signal and the labeled signal is averted and high decoding accuracy and detection sensitivity are guaranteed.

Keywords Suspension array · Gold nanorods · Raman spectroscopy · Surface-enhanced Raman scattering · Encoded micro-quartz pieces

Electronic supplementary material The online version of this article (https://doi.org/10.1007/s00216-019-01929-5) contains supplementary material, which is available to authorized users.

✉ Jingying Jiang
jingyingjiang@buaa.edu.cn

✉ Yonghong He
heyh@sz.tsinghua.edu.cn

[1] School of Precision Instruments & Optoelectronics Engineering, Tianjin University, Tianjin 300072, China

[2] Institute of Optical Imaging and Sensing, Shenzhen Key Laboratory for Minimal Invasive Medical Technologies, Graduate School at Shenzhen, Tsinghua University, Shenzhen 518055, Guangdong, China

[3] Paul C. Lauterbur Research Center for Biomedical Imaging, Shenzhen Institutes of Advanced Technology, Chinese Academy of Sciences, Shenzhen 518055, Guangdong, China

[4] Beijing Advanced Innovation Center for Big Data-Based Precision Medicine, Beihang University, Beijing 100191, China

Introduction

Labeled detection technology and label-free detection technology [1] are the main methods used to detect biomolecules such as proteins and DNA. Due to recent advances in the life sciences and analytical chemistry, methods permitting the high-throughput detection of biomolecules are now urgently required in the field of medical diagnostics [2–5]. Traditional detection methods such as enzyme-linked immunosorbent assays (ELISAs) [6, 7] and chemiluminescence immunoassays [8, 9] are expensive and only allow single-channel analysis. On the other hand, encoded-microcarrier suspension arrays have been found to be very effective methods for multiplex detection, as they are relatively inexpensive, accurate, and sensitive and can be employed for multichannel analysis [10–13]. In these encoded-microcarrier suspension arrays, microbeads are generally used as the microcarriers, and

organic fluorescent dyes and quantum dots (QDs) are frequently used as the encoding materials [14–16]. However, although fluorescence-encoded microbeads are commonly used in multiplex bioassays, the presence of these microbeads complicates the decoding process to some extent due to the ease with which organic fluorescent dyes are quenched and the relatively wide fluorescence peaks of QDs. Thus, while encoded-microbead suspension arrays have many advantages, they also have many limitations.

Compared with fluorescence spectra, Raman spectra are scattering spectra with high spectral resolutions, narrow peaks, and good peak stability. Therefore, suspension arrays based on Raman spectra should, in theory, be more attractive for real-world applications than suspension arrays based on fluorescence spectra [17, 18]. However, the Raman signal intensity is weak and the detection signal can sometimes be submerged in the noise. Hence, it is necessary to enhance the Raman signal. Some researchers have noted that nanometallic structures exhibit plasmon resonance when an electric field is applied, greatly enhancing the signal from the Raman reporter molecules; this is termed the surface-enhanced Raman scattering (SERS) effect [19–22]. Paresh Chandra Ray et al. used gold nanoparticles to create a SERS probe for the detection of trinitrotoluene [23]. In order to maximize the intensity of the Raman signal, it is useful to bind noble metal nanoparticles to the Raman reporter molecules. For example, gold nanoparticles and Raman reporter molecules coupled through Au–S bonds have been used for the quantitative detection and analysis of IgG [24]. Compared with traditional gold nanoparticles, the tunable longitudinal extinction peak and the lightning rod effect of AuNRs result in an enhanced SERS signal [25]. Moreover, the findings of EI-Sayed et al. indicate that AuNR aggregates enhance the SERS signal more than gold nanosphere (AuNS) aggregates under similar experimental conditions [26].

In this paper, we present a novel digital encoding method that is based on AuNR-enhanced Raman spectroscopy and uses micro-quartz pieces (MQPs) as microcarriers. Raman reporter molecules were bound to AuNRs via Au–S chemical bonds to form surface-enhanced Raman scattering labels ("SERS labels"). Various SERS labels were then assembled on the surfaces of MQPs through electrostatic interactions, yielding SERS-label-encoded MQPs, and the Raman spectra of these encoded MQPs were obtained using a Raman spectrometer. Finally, multiplex immunoassay experiments and concentration gradient experiments were performed to analyze the qualitative and quantitative properties of the SERS-label-encoded MQPs, and the detection limit of this novel technique was obtained. In general, Raman spectra have smaller peak half-widths than fluorescence spectra, which provides more space for spectral encoding, thus improving multichannel detection performance. The use of MQPs as carriers eliminates interference arising from background fluorescence, which is an issue when using polystyrene microbeads as carriers. The AuNR-enhanced Raman signal and QD fluorescence are used as the encoded signal and the labeled signal respectively, effectively suppressing any crosstalk between the encoded signal and labeled signal. Meanwhile, as the variety of Raman reporter molecules present is increased, the number of potential codes and thus the coding capacity increase exponentially.

Materials and experiments

Experimental principle

First, a previously reported seed-mediated growth method was used to synthesize the AuNRs. Four Raman reporter molecules with sulfhydryl groups were then selected. These reporter molecules were dissolved completely and mixed with AuNRs, leading to the formation of SERS labels via Au–S bonds. Next, we modified the SERS labels with (3-aminopropyl)triethoxysilane (APTES) to produce surface amino groups. After centrifugation and washing, the SERS labels exhibited positive potential. The MQPs were modified with polyethyleneimine (PEI) and poly(sodium-*p*-styrenesulfonate) (PSS), after which the surfaces of the MQPs were negatively charged. The positively charged SERS labels and the negatively charged MQPs were then combined via electrostatic interactions to obtain the encoded MQPs. Finally, the encoded MQPs were further modified with glutaraldehyde to create aldehyde groups on their surfaces, and IgGs were grafted onto the modified surfaces of the encoded MQPs to act as bioprobes for detecting QD-labeled analytes. Multiplex immunoassay experiments were performed to demonstrate the applicability of this novel suspension array method in biomedicine. Raman decoding of the encoded MQPs was implemented to determine the type of Raman reporter molecules present, and qualitative detection of the analyte was carried out. Fluorescence measurements of the encoded MQPs were conducted, and the analyte was detected quantitatively based on the fluorescence intensity. A schematic of the synthesis and detection of the encoded MQPs is shown in Fig. 1.

Materials

Hydrogen tetrachloroaurate(III) hydrate ($HAuCl_4 \cdot 3H_2O$) and cetyltrimethylammonium bromide (CTAB) were purchased from Sigma–Aldrich (St. Louis, MO, USA). Sodium borohydride ($NaBH_4$) was purchased from Damao Chemical Reagent Factory (Tianjin, China). Silver nitrate ($AgNO_3$) was purchased from Sinopharm Chemical Reagent Co., Ltd. (Shanghai, China). Ascorbic acid (AA) was purchased from Aladdin Biochemical Technology Co., Ltd. (Shanghai, China). Polyethyleneimine (PEI), poly(sodium-*p*-styrenesulfonate) (PSS), (3-

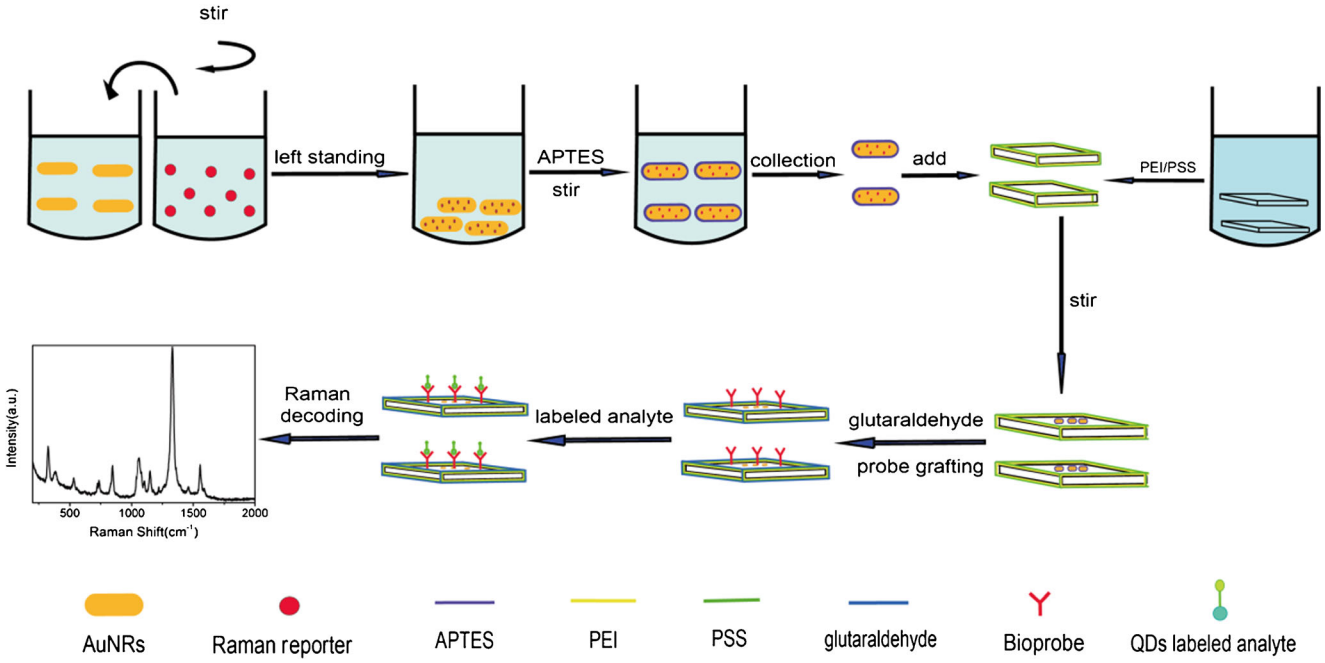

Fig. 1 Principle of the novel digital encoding method that is based on AuNR-enhanced Raman spectroscopy and uses micro-quartz pieces (MQPs) as microcarriers, and the procedure employed to synthesize the encoded MQPs

aminopropyl)triethoxysilane (APTES), 2-naphthalenethiol (2-NT), 4-chlorothiophenol (4-CBT), 4-mercaptophenol (4-HBT) and 5,5′-dithiobis-(2-nitrobenzoic acid) (DTNB) were purchased from Shanghai Macklin Biochemical Co., Ltd. (Shanghai, China). Phosphate-buffered saline (PBS) was purchased from Beijing Solarbio Science & Technology Co., Ltd. (Beijing, China). Sodium chloride (NaCl) was purchased from Tianjin Zhiyuan Reagent Co., Ltd. (Tianjin, China). Non-protein blocking solution was purchased from Beijing Bai'aolaibo Technological Development Corporation (Beijing, China). Three types of IgGs (mouse, rabbit, and human) were purchased from Bioss Biotechnology (Beijing, China). Three types of QD-labeled anti-IgGs (goat anti-mouse IgG labeled with 565-nm QDs, goat anti-rabbit IgG labeled with 585-nm QDs, and goat anti-human IgG labeled with 610-nm QDs) were purchased from NajingTech Co., Ltd. (Hangzhou, China).

Characterization

Scanning electron microscopy (SEM) was performed with a Supra 55 instrument (Carl Zeiss, Jena, Germany). Transmission electron microscopy (TEM) was carried out with an FEI (Hillsboro, OR, USA) Tecnai Spirit T12. Zeta potentials were measured on a Zetasizer Nano ZS90 (Malvern Instruments, Malvern, UK). Raman spectra were recorded using a confocal Raman microscope (LabRAM HR800, HORIBA, Kyoto, Japan) with a 50× microscope objective and laser-induced excitation at 785 nm. The acquisition time was 5 s, and two repetitions were performed per spectrum. The laser power of the Raman microscope used in the acquisition was 7.8 mW, and the spectral resolution was 2 cm^{-1}.

Synthesis of gold nanorods

CTAB-stabilized AuNRs were synthesized using a previously reported seed-mediated growth method that involves seed synthesis and continuous seed growth [27, 28]. In brief, 4 mL of 100 mM CTAB solution, 40 μL of 24.28 mM $HAuCl_4$, and 24 μL of 100 mM $NaBH_4$ freshly prepared in ice water were added to a 50-mL round-bottom flask and stirred for 90 s to prepare the AuNR seed solution. The growth solution was prepared by adding 20 mL of 0.2 M CTAB solution, 400 μL of 24.28 mM $HAuCl_4$ solution, 150 μL of 5 M HCl, as well as 50 μL of 40 mM $AgNO_3$ solution and 160 mL of 0.1 M AA to a 50-mL round-bottom flask at intervals of 2 min. The $AgNO_3$ was added to adjust the aspect ratio of the synthesized AuNRs. Lastly, 28 μL of the seed solution were added to the growth solution and the mixture was stirred for 30 s. Finally, the flask was left standing in an incubator at 30 °C for 12 h, during which time the mixture turned blue, indicating the formation of AuNRs. For more information on this, please refer to the section "The synthesis of gold nanorods" in the "Electronic supplementary material" (ESM).

Synthesis of surface-enhanced Raman scattering labels

SERS labels were obtained by coupling the Raman reporter molecules with AuNRs via Au–S chemical bonds (see the

"Synthesis of surface enhanced Raman scattering labels" section in the ESM) [29, 30]. Firstly, 10 mL of freshly synthesized AuNRs were centrifuged twice and redispersed in 1 mL of ethanol for subsequent use. A certain mass of Raman reporter molecules was then weighed and dissolved in 2 ml of ethanol at a concentration of 0.3 mol/L. After the Raman reporter molecules had completely dissolved, they were mixed with the AuNRs that had been dissolved in ethanol for 2 h. This mixture was left to stand overnight in a fume hood to allow the Raman reporter molecules to bind to the AuNRs and thus obtain SERS labels. In this work, we used four different Raman reporter molecules: 2-NT, 4-CBT, 4-HBT, and DTNB. Au–S chemical bonds formed spontaneously between the selected sulfhydryl Raman reporter molecules and the AuNRs. After the mixture had been left overnight, the supernatant was removed and the precipitate was washed by centrifugation several times to acquire the SERS labels. A comparison of the results of standard Raman spectroscopy and enhanced Raman spectroscopy using the four Raman reporter molecules is shown in Fig. S1 of the ESM.

Conjugation of the SERS labels and micro-quartz pieces

In our experiments, micro-quartz pieces (MQPs) about 100 μm in side length were used as microcarriers. The MQPs and the SERS labels were combined via electrostatic interactions (see the "Conjugation of SERS labels and micro-quartz pieces" section in the ESM). Briefly, this experimental process involved three specific operations. First, the SERS labels were functionalized by mixing them with 3 mL of a 50% (v/v) APTES ethanol solution for 2 h at room temperature to obtain amino-functionalized SERS labels with positively charged surfaces [31]. After centrifuging twice and removing the supernatant, the precipitate was dissolved in 1 mL of deionized water and saved for subsequent use. Second, the MQPs (5000 pieces) were modified by a layer-by-layer self-assembly method. Specifically, the MQPs were soaked in piranha solution to have hydroxyl groups on its surface and enhance the hydrophilicity, and then washed with deionized water to remove the piranha solution. Next, the MQPs were dispersed in 1.5 mL of 6.7 mmol/L PEI solution (4 mg / mL, 0.5 M sodium chloride solution) and stirred for 1 hour to ensure that the MQPs were positively charged. After washing with deionized water five times, the MQPs were redispersed in 1.5 mL of 0.025 mmol/L PSS solution (2 mg/mL, 0.5 M sodium chloride solution) and stirred for 1 h to create a negatively charged surface environment. Then, the MQPs were redispersed in 500 μL of deionized water and amino-functionalized SERS labels were added. Third, the mixture solution was stirred at room temperature for 1.5 h to obtain the final SERS-label-encoded MQPs. It is worth noting that the positively charged surfaces of the SERS labels allowed them to react directly with the MQPs, which had negatively charged surfaces. The time required from the start of the synthesis of the AuNRs to the final synthesis of encoded MQPs was 25.5–27.5 h

Application of SERS-label-encoded MQPs to the detection of target biomolecules

In order to demonstrate the potential of the SERS-label-encoded MQPs for high-throughput biomolecule detection, we grafted probe molecules onto the surfaces of the encoded MQPs and carried out a series of antigen–antibody binding experiments [32, 33]. The three Raman reporter molecules we used in these experiments were 2-NT, 4-CBT, and DTNB, which were combined in different ways. In the multiplex immunoassay experiments, we prepared three different types of SERS-label-encoded MQPs: MQPs-AuNRs-DTNB ("MQPs1"), MQPs-AuNRs-(2-NT) ("MQPs2"), and MQPs-AuNRs-(DTNB+4-CBT) ("MQPs3"). These three kinds of encoded MQPs were then mixed with 1.5 mL of a 5% glutaraldehyde [34, 35] solution for 1 h at room temperature and washed with PBS solution. Thereafter, 200 μL of rabbit IgG (1 mg/mL), 200 μL of mouse IgG (1 mg/mL), or 200 μL of human IgG (1 mg/mL) were added to the three types of encoded MQPs, respectively, and the mixtures were stirred at 37 °C for 2 h in an incubator. After completing the reaction, they were washed several times with PBS solution before 1.5 mL of non-protein blocking solution were added and the mixtures were stirred for 8 h at 4 °C in order to block the amino groups that did not participate in the reaction. Finally, QD-labeled anti-IgGs (25 nM goat anti-mouse IgG labeled with 565-nm QDs, 15 nM goat anti-rabbit IgG labeled with 585-nm QDs, and 8 nM goat anti-human IgG labeled with 610-nm QDs) were mixed with PBS solution to create a sample, and the three types of IgG-conjugated MQP solutions were simultaneously added to the sample and allowed to react with the QD-labeled anti-IgGs in an incubator at 37 °C for 1 h. To remove the unreacted QD-labeled anti-IgGs, the MQPs were washed with PBS solution several times and redispersed in deionized water. To assess the concentration response of the encoded MQPs, we performed a concentration gradient experiment. For quantitative analysis, goat anti-mouse IgG labeled with 565-nm QDs was used as the analyte at concentrations of 0, 0.46875, 0.9375, 1.875, 3.75, 7.5, 15, and 30 nM in order to demonstrate the concentration response of MQPs1. For more information about this, refer to the "Application of SERS labels encoded MQPs in biomolecule detection" section of the ESM.

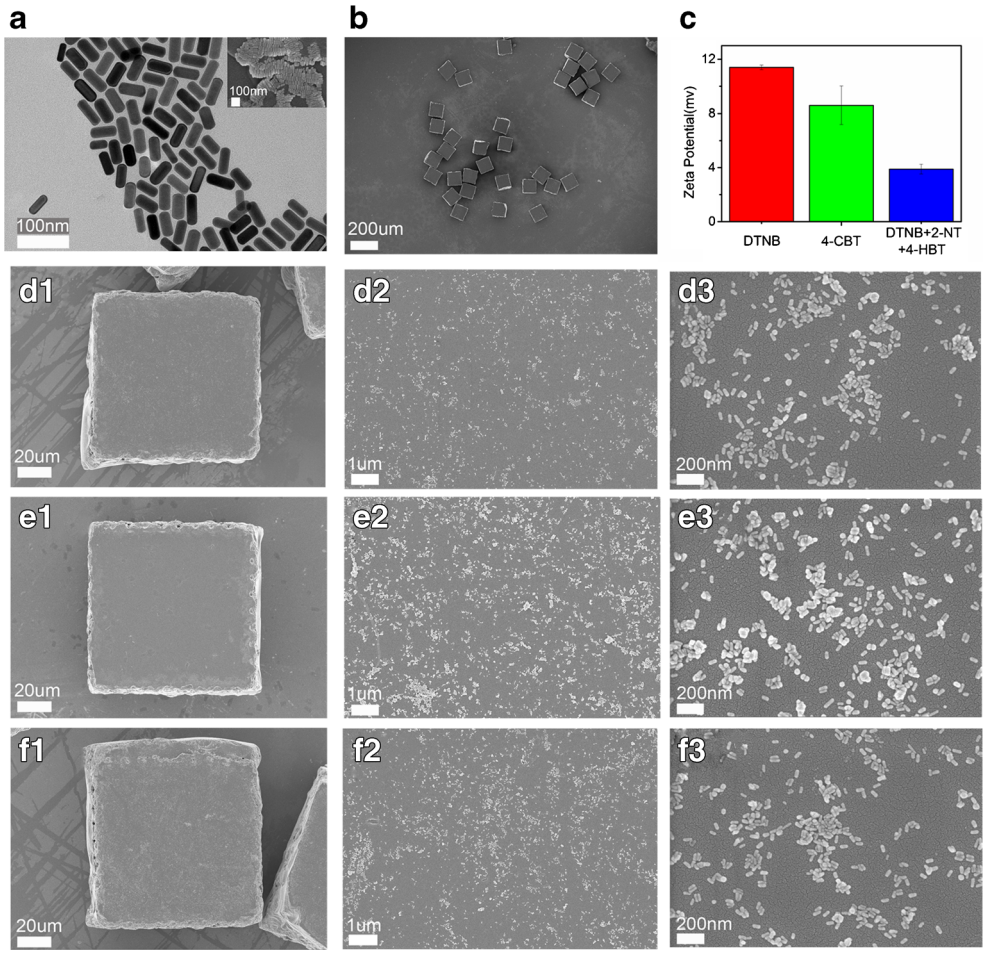

Fig. 2 **a** TEM image of AuNRs (*scale bar*: 100 nm). The *inset* shows a SEM image of AuNRs (*scale bar*: 100 nm). **b** SEM image of the initial MQPs at low magnification. **c** The zeta potentials of various SERS labels. **d** SEM images of DTNB-encoded MQPs at different magnifications. **e** SEM images of (DTNB + 4-HBT)-encoded MQPs at different magnifications. **f** SEM images of (DTNB + 4-CBT + 4-HBT)-encoded MQPs at different magnifications

Results and discussion

Characterization of the AuNRs and the SERS-label-encoded MQPs

The nanoparticles we used in the experiment were AuNRs, and TEM and SEM images of the AuNRs we synthesized are shown in Fig. 2a. It is clear from this image that the AuNRs have a rod-like structure, and they are arranged neatly and compactly before they are reacted with other chemical substances. Figure 2b shows a SEM image of blank MQPs at low magnification. The image shows the square structure of the MQPs. Figure 2c illustrates the electrical properties of the SERS labels in aqueous solution. From the histograms shown in the figure, it is clear that the APTES-modified SERS labels are positively charged. A TEM image of APTES-coated AuNRs is shown in the ESM (Fig. S3). In previous studies, PEI and PSS have often been used as cationic surfactants and anionic surfactants, leading to a positively or negatively charged surface of the material being modified. In our experiments, the surfaces of the MQPs were modified with PEI and then PSS, leading to negatively charged MQP surfaces. We found that SERS labels can be assembled on the surfaces of these negatively charged MQPs. When the AuNRs were combined with the four Raman reporter molecules and assembled on the surfaces of the MQPs via electrostatic interactions, we obtained 15 types of SERS-label-encoded MQPs. SEM images of three types of encoded MQPs are shown in Fig. 2d–f. Figure 2d shows a SEM image of DTNB-encoded MQPs, which were obtained by combining DTNB with AuNRs and assembling the resulting SERS labels on the surfaces of MQPs. Figure 2e shows a SEM image of the (DTNB + 4-HBT)-encoded MQPs, obtained by simultaneously reacting DTNB and 4-HBT with AuNRs and combining the resulting SERS labels with MQPs. Figure 2f presents a SEM image of (DTNB + 4-CBT + 4-HBT)-encoded MQPs, which were acquired by simultaneously assembling DTNB, 4-CBT, and 4-HBT on the surfaces of AuNRs to form SERS labels, and then combining these SERS labels with MQPs. The above results and analysis confirm that SERS labels can be assembled on the surfaces of the MQPs, and that the synthesis of SERS-label-encoded MQPs using our method is feasible and effective.

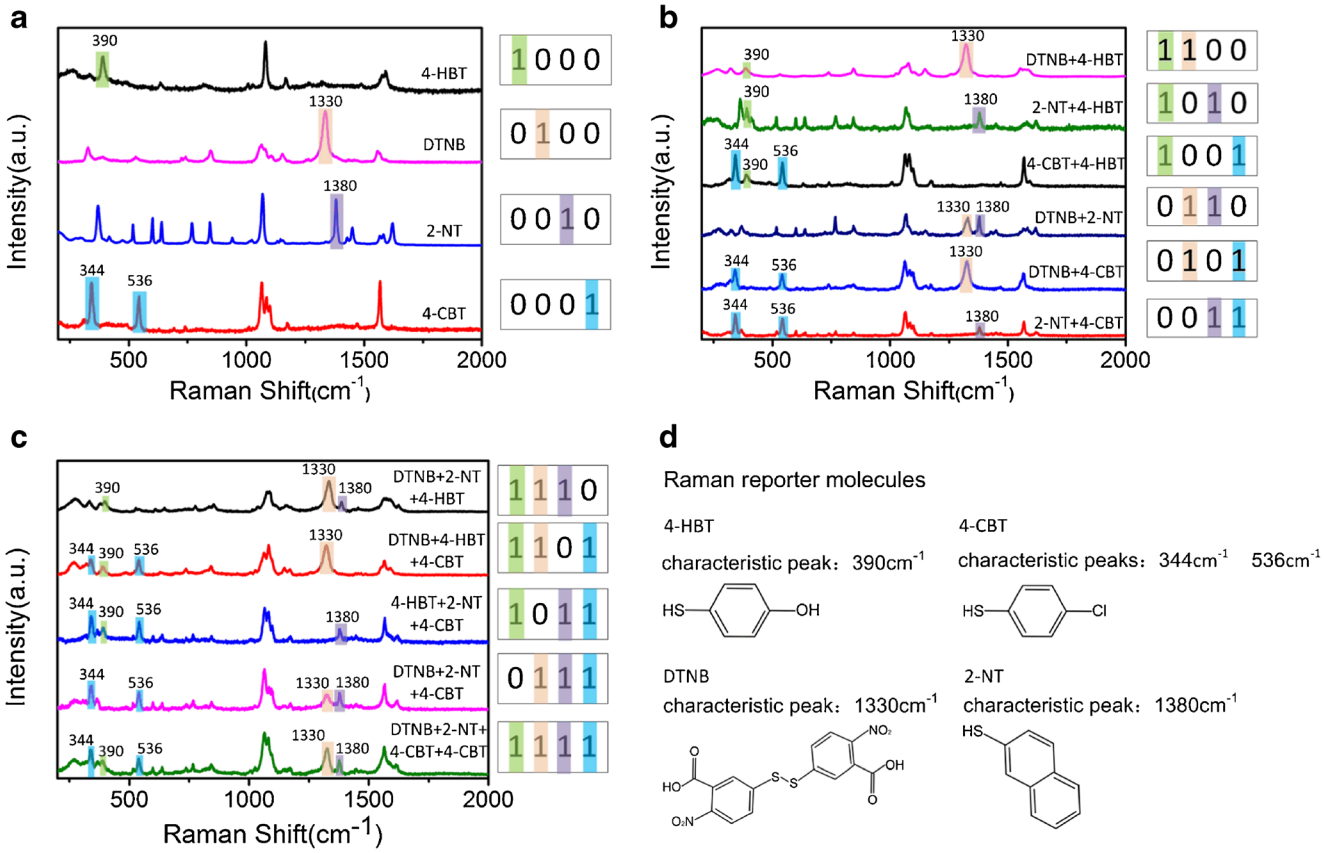

Fig. 3 **a** Typical Raman spectra (*left*) of MQPs encoded with four kinds of Raman reporter molecules and their corresponding binary digit sequences (1000, 0100, 0010, 0001; *right*). **b** Raman spectra (*left*) of MQPs encoded with two types of Raman reporter molecules and their corresponding binary digit sequences (1100, 1010, 1001, 0110, 0101, 0011; *right*). **c** Raman spectra (*left*) of MQPs encoded with three or four types of Raman reporter molecules and their corresponding binary digit sequences (1110, 1101, 1011, 0111, 1111; *right*). **d** The structural formulae of the four kinds of Raman reporter molecules, and selected characteristic peaks for those molecules. All Raman spectra were subjected to baseline removal and normalization

Raman spectra and digital transformation of the SERS-label-encoded MQPs

Using the four different Raman reporter molecules and combinations of them, we prepared 15 different types of SERS-label-encoded MQPs, which were examined by optical microscopy and characterized by confocal Raman microscopy. These four Raman reporter molecules were 4-HBT, DTNB, 2-NT, and 4-CBT, and the Raman spectra and structural formulae of these molecules are presented in Fig. 3a and d. The shaded regions of the curves in Fig. 3a indicate characteristic peaks of these four Raman reporter molecules, which are located at 390, 1330, 1380, and, 344 and 536 cm^{-1}, respectively (the positions of these characteristic peaks are also provided in Fig. 3d). These peaks can be used to distinguish between the four Raman reporter molecules, so long as the peaks are separated by at least 20 cm^{-1} in the Raman spectrum. The four Raman reporter molecules were mixed in different ways and combined with AuNRs to obtain SERS labels, which yielded 15 types of SERS-label-encoded MQPs. The 15 Raman spectra for these 15 types of encoded MQPs are shown in Fig. 3a–c.

We created a digital transformation map and obtained 15 sets of binary digit sequences [36] that could be used to distinguish the encoded MQPs. Color shading is used in Fig. 3a–c to indicate the position(s) of a characteristic peak (or multiple such peaks) in the Raman spectra of the encoded MQPs. "1" was used to denote that a particular characteristic peak was present in the Raman spectrum, whereas "0" indicated the absence of that peak. It should be noted that the number of possible codes increases exponentially with the number of encoding materials when this coding and digital conversion method is applied. Suppose we use n encoding materials, then the number of potential codes can be obtained using the following formula:

$$w = C_n^1 + C_n^2 + \ldots + C_n^n = 2^n - 1.$$

Here, w is the number of possible codes. In practical applications, the number of available codes is actually lower than w due to, for example, background peaks; however, the approximately exponential increase in the number of codes with n can still provide sufficiently

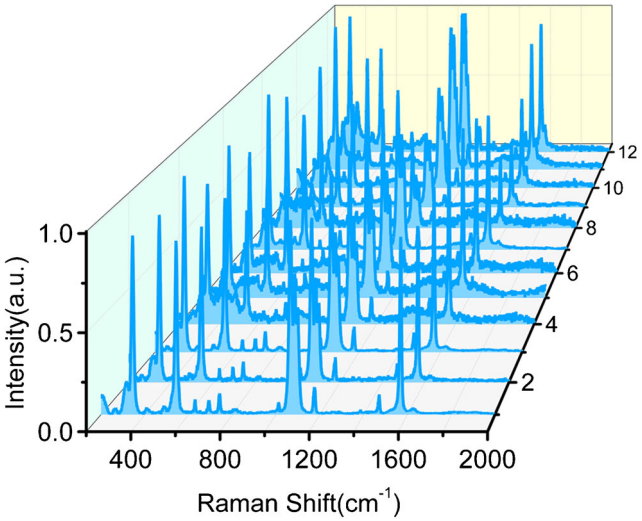

Fig. 4 Comparison of the characteristic peak positions (344 cm^{-1} and 536 cm^{-1}) in Raman spectra of 4-CBT-encoded MQPs obtained at 12 points within the same sample

large coding libraries to enable high-throughput biomolecule detection based on Raman spectral features, so this approach is widely used in multichannel analysis and detection. Figure 3a shows the Raman spectra of MQPs encoded with one type of Raman reporter molecule plus AuNRs, as well as the binary sequence obtained by digital conversion method; Fig. 3b shows the same for MQPs encoded with mixtures of two kinds of Raman reporter molecules plus AuNRs. It can be seen in Fig. 3b that the spectra obtained from the encoded MQPs contain characteristic peaks of two types of Raman reporter molecules. Six binary digit sequences were obtained in this case: 1100, 1010, 1001, 0110, 0101, and 0011. The Raman spectra obtained when MQPs were encoded with mixtures of three or four Raman reporter molecules plus AuNRs, leading to five SERS labels, are shown in Fig. 3c, as are the corresponding binary digit sequences. (Note that the spectrum of MQPs encoded with DTNB, 2-NT, and 4-HBT plus AuNRs is provided in Fig. S2 of the ESM.) In Fig. 3c, we can clearly distinguish the characteristic peaks of the encoded MQPs, allowing us to infer the Raman reporter molecules present.

Taking the spectral detection of 4-CBT-encoded MQPs as an example, we obtained Raman spectra at multiple test points in the same sample, which the test points of the samples were randomly selected on the surface of the MQPs, as Fig. 4 shows. It is clear that the characteristic peaks of 4-CBT at 344 cm^{-1} and 536 cm^{-1} can be seen in all of the Raman spectra obtained at 12 positions in the sample. Thus, the spectrum of the encoded MQPs shows excellent reproducibility, and the results indicate that our method is effective.

Application of SERS-label-encoded MQPs to biomolecule detection

To further demonstrate the feasibility of using encoded MQPs for biomolecule detection, we prepared three different types of SERS-label-encoded MQPs for multiplex protein detection: MQPs1 (MQPs-AuNRs-DTNB), MQPs2 (MQPs-AuNRs-(2-NT)), and MQPs3 (MQPs-AuNRs-(DTNB+4-CBT)), which bind to mouse IgG, rabbit IgG, and human IgG, respectively. We also prepared a sample containing three different QD-labeled anti-IgGs: goat anti-mouse IgG labeled with 565-nm QDs, goat anti-rabbit IgG labeled with 585-nm QDs, and goat anti-human IgG labeled with 610-nm QDs. The three types of IgG-grafted encoded MQPs were then added to the sample solution and left to react for a period of time. The reacted MQPs were placed on a glass slide and examined via fluorescence microscopy; see Fig. 5a. Figure 5b is a photograph obtained under a Raman microscope of the same reacted MQPs shown in Fig. 5a. The decoded Raman spectra for the three MQPs circled in Fig. 5b are shown in Fig. 5c. Note that the colors used for the Raman spectra correspond to the colors of the circles in Fig. 5b: the red, blue, and black circles indicate MQPs containing DTNB, 2-NT, and DTNB + 4-CBT, respectively. These Raman decoding results are consistent with the labeled antibody species, indicating that the encoded MQPs can capture specific antibodies, as shown

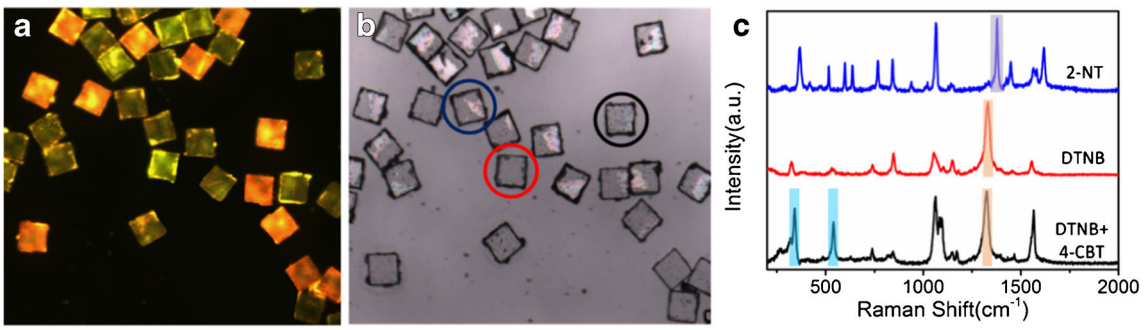

Fig. 5 **a** Fluorescence microscopy image of a mixed suspension array used in multiplexed analysis. **b** Raman microscopy image of the same mixed suspension array. **c** Decoded Raman spectra of three of the reacted MQPs (*circled*)

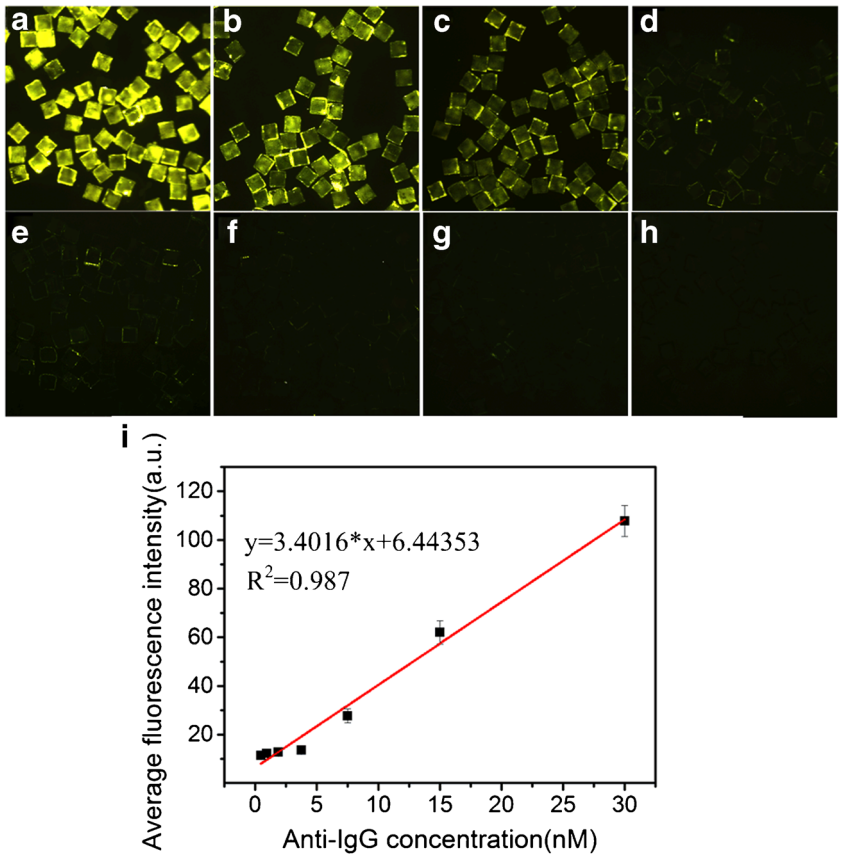

Fig. 6 **a**–**h** Images showing the fluorescence generated by the reaction of the analyte with MQPs1 at analyte concentrations of 30, 15, 7.5, 3.75, 1.875, 0.9375, 0.46875 and 0, respectively. Size of field of view: 1.26 mm × 1.26 mm. **g** Concentration–response curve for the reacted MQPs1

in Fig. 5. Therefore, biomolecules can be specifically detected by encoded MQPs synthesized using our method.

The ability of the fluorescence imaging pathway to perform quantitative analysis was confirmed by carrying out concentration gradient experiments. We selected goat anti-mouse IgG labeled with 565-nm QDs as the analyte to be quantitatively analyzed at concentrations of 0, 0.46875, 0.9375, 1.875, 3.75, 7.5, 15, and 30 nM in order to verify the concentration response of a MQPs1-based suspension array. The results of the concentration gradient experiment (5000 MQPs were used with each concentration of analyte) are shown in Fig. 6. Figure 6a–h show fluorescence images of a group of analyte-bound MQPs1. We can see that the average fluorescence intensity of the image decreases in the order a–h, and the analyte concentrations that yield the eight images are 30, 15, 7.5, 3.75, 1.875, 0.9375, 0.46875, and 0 nM, respectively. Figure 6i shows a plot of the average fluorescence intensity of the reacted MQPs versus the analyte concentration, along with a linear fit to the data points. We can see that the average measured fluorescence intensity of the MQPs varies linearly with analyte concentration within a certain concentration interval. The detection limit, obtained by calculating three times the standard deviation and using the fluorescence intensity of the blank sample, was calculated to be 1.78 nM. We know that there is a correlation between the detection limit and the fluorescence intensity of the label. Utilizing QD labels with higher quantum yields allows us to access lower detection limits and better performance.

Conclusions

In conclusion, we developed a facile and multiplex digital coding method based on the use of AuNR-enhanced Raman spectroscopy and MQPs to achieve the detection of biomolecules. We utilized four kinds of Raman reporter molecules to obtain 15 different coding combinations and 15 binary digit sequences of the encoded MQPs. Because the Raman spectrum is independent of the fluorescence spectrum, crosstalk between the encoded signal and the label signal can be avoided. The use of MQPs as carriers can also eliminate interference from background fluorescence, which is an issue when using polystyrene microbeads for example. In addition, quantifying the fluorescence of MQPs using fluorescence microscopy has the advantages of being simple, fast, and inexpensive. At the same time, the number of codes increases exponentially as more and more types of Raman reporter molecules are included, thus augmenting the coding capacity. Therefore, it is feasible to utilize this method to achieve the multiplex detection of proteins, meaning that the method has good potential real-world applicability and could be applied to biomolecule detection.

Acknowledgements Financial support from the Tianjin Applied Basic and Frontier Technology Research Program (16JCZDJC31200), the National Science Foundation of China (NSFC) (61875102, 61675113, 61527808), and the Science and Technology Research Program of Shenzhen City (JCYJ20170412170255060, JCYJ20160324163759208, JCYJ20170412171856582, JCYJ20170816161836562, JCYJ20170817111912585) is acknowledged.

Compliance with ethical standards

Conflict of interest The authors declare that they have no conflict of interest.

References

1. Pittner A, Wendt S, Zopf D, Dathe A, Grosse N, Csáki A, et al. Fabrication of micro-patterned substrates for plasmonic sensing by piezo-dispensing of colloidal nanoparticles. Anal Bioanal Chem. 2019;411(8):1537–47. https://doi.org/10.1007/s00216-019-01587-7.
2. Schlücker S. SERS microscopy: nanoparticle probes and biomedical applications. Chemphyschem. 2009;10(9-10):1344–54. https://doi.org/10.1002/cphc.200900119.
3. Ng P, Tan JJ, Ooi HS, Lee YL, Chiu KP, Fullwood MJ, et al. Multiplex sequencing of paired-end ditags (MS-PET): a strategy for the ultra-high-throughput analysis of transcriptomes and genomes. Nucleic Acids Res. 2006;34(12):e84. https://doi.org/10.1093/nar/gkl444.
4. Chen L, Wang Y, Fu X, Chen L. Surface-enhanced Raman scattering nanoprobes. In: Chen L, Wang Y, Fu X, Chen L, editors. Novel optical nanoprobes for chemical and biological analysis. Berlin: Springer; 2014. p. 75–95. https://doi.org/10.1007/978-3-662-43624-0_4.
5. Xie J, Zhang Q, Lee JY, Wang DIC. The synthesis of SERS-active gold nanoflower tags for in vivo applications. ACS Nano. 2008;2(12):2473–80. https://doi.org/10.1021/nn800442q.
6. Rennard SI, Berg R, Martin GR, Foidart JM, Robey PG. Enzyme-linked immunoassay (ELISA) for connective tissue components. Anal Biochem. 1980;104(1):205–14. https://doi.org/10.1016/0003-2697(80)90300-0.
7. Engvall E, Perlmann P. Enzyme-linked immunosorbent assay (ELISA) quantitative assay of immunoglobulin G. Immunochemistry. 1971;8(9):871–4. https://doi.org/10.1016/0019-2791(71)90454-X.
8. Bowie AR, Sanders MG, Worsfold PJ. Analytical applications of liquid phase chemiluminescence reactions—a review. J Biolumin Chemilumin. 1996;11(2):61–90. https://doi.org/10.1002/(sici)1099-1271(199603)11:2<61::aid-bio406>3.0.co;2-o.
9. Fähnrich KA, Pravda M, Guilbault GG. Recent applications of electrogenerated chemiluminescence in chemical analysis. Talanta. 2001;54(4):531–59. https://doi.org/10.1016/S0039-9140(01)00312-5.
10. Zhang Z, Long Y, Pan J, Yan X. Preparation of fluorescence-encoded microspheres in a core–shell structure for suspension arrays. J Mater Chem. 2010;20(6):1179–85. https://doi.org/10.1039/B919955A.
11. Wilson R, Cossins AR, Spiller DG. Encoded microcarriers for high-throughput multiplexed detection. Angew Chem Int Ed Engl. 2006;45(37):6104–17. https://doi.org/10.1002/anie.200600288.
12. Long Y, Zhang Z, Yan X, Xing J, Zhang K, Huang J, et al. Multiplex immunodetection of tumor markers with a suspension array built upon core–shell structured functional fluorescence-encoded microspheres. Anal Chim Acta. 2010;665(1):63–8. https://doi.org/10.1016/j.aca.2010.03.009.
13. He Q, Guan T, He Y, Lu B, Li D, Chen X, et al. Digital encoding based molecular imprinting suspension array for multiplexed label-free sensing of phenol derivatives. Sens Actuators B: Chem. 2018;271:367–73. https://doi.org/10.1016/j.snb.2018.05.101.
14. Gao Y, Stanford WL, Chan WCW. Quantum-dot-encoded microbeads for multiplexed genetic detection of non-amplified DNA samples. Small. 2010;7(1):137–46. https://doi.org/10.1002/smll.201000909.
15. Mattheakis LC, Dias JM, Choi Y-J, Gong J, Bruchez MP, Liu J, et al. Optical coding of mammalian cells using semiconductor quantum dots. Anal Biochem. 2004;327(2):200–8. https://doi.org/10.1016/j.ab.2004.01.031.
16. Zhao Y, Shum HC, Chen H, Adams LLA, Gu Z, Weitz DA. Microfluidic generation of multifunctional quantum dot barcode particles. J Am Chem Soc. 2011;133(23):8790–3. https://doi.org/10.1021/ja200729w.
17. Cao YC, Jin R, Mirkin CA. Nanoparticles with Raman spectroscopic fingerprints for DNA and RNA detection. Science (New York, NY). 2002;297(5586):1536–40. https://doi.org/10.1126/science.297.5586.1536.
18. Cho H, Lee B, Liu GL, Agarwal A, Lee LP. Label-free and highly sensitive biomolecular detection using SERS and electrokinetic preconcentration. Lab Chip. 2009;9(23):3360–3. https://doi.org/10.1039/b912076a.
19. Lee S, Joo S, Park S, Kim S, Kim HC, Chung TD. SERS decoding of micro gold shells moving in microfluidic systems. Electrophoresis. 2010;31(10):1623–9. https://doi.org/10.1002/elps.200900743.
20. Kneipp K, Wang Y, Kneipp H, Perelman LT, Itzkan I, Dasari RR, et al. Single molecule detection using surface-enhanced Raman scattering (SERS). Phys Rev Lett. 1997;78(9):1667–70. https://doi.org/10.1103/PhysRevLett.78.1667.
21. Schlücker S. Surface-enhanced Raman spectroscopy: concepts and chemical applications. Angew Chem Int Ed Engl. 2014;53(19):4756–95. https://doi.org/10.1002/anie.201205748.
22. Liu B, Zhao X, Jiang W, Fu D, Gu Z. Multiplex bioassays encoded by photonic crystal beads and SERS nanotags. Nanoscale. 2016;8(40):17465–71. https://doi.org/10.1039/c6nr05588e.
23. Dasary SSR, Singh AK, Senapati D, Yu H, Ray PC. Gold nanoparticle based label-free SERS probe for ultrasensitive and selective detection of trinitrotoluene. J Am Chem Soc. 2009;131(38):13806–12. https://doi.org/10.1021/ja905134d.
24. Yap LW, Chen H, Gao Y, Petkovic K, Liang Y, Si KJ, et al. Bifunctional plasmonic-magnetic particles for an enhanced microfluidic SERS immunoassay. Nanoscale. 2017;9(23):7822–9. https://doi.org/10.1039/c7nr01511a.
25. Orendorff CJ, Gole A, Sau TK, Murphy CJ. Surface-enhanced Raman spectroscopy of self-assembled monolayers: sandwich architecture and nanoparticle shape dependence. Anal Chem. 2005;77(10):3261–6. https://doi.org/10.1021/ac048176x.
26. Nikoobakht B, El-Sayed MA. Surface-enhanced Raman scattering studies on aggregated gold nanorods. J Phys Chem A. 2003;107(18):3372–8. https://doi.org/10.1021/jp026770+.
27. Duan J, Park K, MacCuspie RI, Vaia RA, Pachter R. Optical properties of rodlike metallic nanostructures: insight from theory and experiment. J Phys Chem C. 2009;113(35):15524–32. https://doi.org/10.1021/jp902448f.
28. Li G, Zhu L, Wu Z, He Y, Tan H, Sun S. Digital concentration readout of DNA by absolute quantification of optically countable gold nanorods. Anal Chem. 2016;88(22):10994–1000. https://doi.org/10.1021/acs.analchem.6b02712.
29. Jiang L, Qian J, Cai F, He S. Raman reporter-coated gold nanorods and their applications in multimodal optical imaging of cancer cells. Anal Bioanal Chem. 2011;400(9):2793. https://doi.org/10.1007/s00216-011-4894-6.

30. Wu L, Wang Z, Zong S, Huang Z, Zhang P, Cui Y. A SERS-based immunoassay with highly increased sensitivity using gold/silver core-shell nanorods. Biosens Bioelectron. 2012;38(1):94–9. https://doi.org/10.1016/j.bios.2012.05.005.
31. Tsukruk VV, Bliznyuk VN, Visser D, Campbell AL, Bunning TJ, Adams WW. Electrostatic deposition of polyionic monolayers on charged surfaces. Macromolecules. 1997;30(21):6615–25. https://doi.org/10.1021/ma961897g.
32. Shen Z, He Y, Zhang G, He Q, Li D, Ji Y. Dual-wavelength digital holographic phase and fluorescence microscopy for an optical thickness encoded suspension array. Opt Lett. 2018;43(4):739–42. https://doi.org/10.1364/ol.43.000739.
33. He Q, Li D, He Y, Guan T, Zhang Y, Shen Z, et al. Optical demodulation system for digitally encoded suspension array in fluoroimmunoassay. J Biomed Opt. 2017;22(9):1–7. https://doi.org/10.1117/1.jbo.22.9.097003.
34. Pauliukaite R, Ghica ME, Fatibello-Filho O, Brett CMA. Comparative study of different cross-linking agents for the immobilization of functionalized carbon nanotubes within a chitosan film supported on a graphite−epoxy composite electrode. Anal Chem. 2009;81(13):5364–72. https://doi.org/10.1021/ac900464z.
35. Sharma R (2015) Glutaraldehyde sandwiched amino functionalised polymer based aptasensor for the determination and quantification of chloramphenicol. RSC Adv. 2015;5:69356–64 https://doi.org/10.1039/c5ra11131e.
36. Lai Y, Sun S, He T, Schlücker S, Wang Y (2015) Raman-encoded microbeads for spectral multiplexing with SERS detection. RSC Adv. 2015;5:13762–7. https://doi.org/10.1039/C4RA16163G.